SCIENCE CHINA
Information Sciences

• RESEARCH PAPER •

January 2025, Vol. 68, Iss. 1, 112205:1–112205:14
https://doi.org/10.1007/s11432-023-4182-6

Dynamic event-triggered data-driven iterative learning bipartite tracking control for nonlinear MASs with prescribed performance

Tao SHI[1] & Wei-Wei CHE[2,3*]

[1]*School of Mechatronic Engineering and Automation, Shanghai University, Shanghai 200444, China;*
[2]*State Key Laboratory of Synthetical Automation for Process Industries, Northeastern University, Shenyang 110819, China;*
[3]*College of Information Science and Engineering, Northeastern University, Shenyang 110819, China*

Received 18 September 2023/Revised 16 March 2024/Accepted 4 August 2024/Published online 26 December 2024

Abstract This article proposes a distributed dynamic event-triggered data-driven iterative learning control (DET-DDILC) scheme under a predefined performance to tackle the bipartite tracking control problem for multiagent systems (MASs). An improved dynamic linearization technique is utilized to convert the nonlinear MASs into an iterative linear data model. First, a peer-to-peer mapping function is introduced to map the constrained distributed system output homeomorphism to an unconstrained one. In addition, a DET mechanism based on a time-iteration-varying function is devised to conserve network communication resources. Based on the unconstrained transformation and the designed DET mechanism, the DET-DDILC algorithm is devised to ensure that the bipartite tracking performance of MASs can be within the preset range. Finally, the effectiveness and feasibility of the designed control scheme are demonstrated via a simulation case by a comparison.

Keywords bipartite tracking control, prescribed performance, event-triggered, iterative learning control, multiagent systems

Citation Shi T, Che W-W. Dynamic event-triggered data-driven iterative learning bipartite tracking control for nonlinear MASs with prescribed performance. Sci China Inf Sci, 2025, 68(1): 112205, https://doi.org/10.1007/s11432-023-4182-6

1 Introduction

Recently, the distributed cooperative control of multiagent systems (MASs) has gained considerable attention because of its practicability and broad applications in various fields, such as robotics [1], aerospace [2], and transportation [3]. MASs consist of multiple agents that interact with each other to achieve specific objectives through collaboration and coordination. Various collaborative control methods have been proposed for MASs, including leader-following consensus control, leaderless consensus control, and competitive-cooperative consensus control. The leader-following consensus control typically involves designating one or more leaders to coordinate the behavior of the group. In this case, leaders usually have global information to make decisions and guide the behavior of other agents [4–10]. For instance, in Liu et al. [11], the leader-following control problem under a class of reinforcement learning game algorithms was studied. Consequently, leaderless consensus control is based on each agent making decisions independently and collaborating with others to achieve system goals. In this case, agents usually only know local information and must establish connections between agents through topology [12–16]. For example, Hu et al. [17] tackled a class of typical symmetric bimatrix game problems under Q-learning algorithms on multi-ple agents.

The existing literature on MASs often assumes that agents only have collaborative relationships with each other. However, in reality, agents can have a mixture of cooperative and competitive relationships, similar to trust or distrust relationships in social networks. Therefore, studying MASs with the coexistence of cooperation and competition is of practical and theoretical significance. One intriguing problem that arises from this balance between cooperation and competition is the bipartite tracking control in MASs. For this bipartite tracking control problem, agents within the same subset exhibit cooperative relationships, whereas those outside of the subset exhibit competitive relationships. Relevant research on

* Corresponding author (email: cwwemail1980@126.com)

this topic can be found in previous studies [18–25]. For instance, cooperative-competitive relationships on a class of societies were investigated previously [22–24] by modeling social relationships among humans.

Because agents interact with each other through communication networks in MASs, therefore, ensuring the reliability of communication networks while saving communication resources is crucial. In this respect, the event-triggered mechanism (ETM) can ensure that corresponding operations are executed as long as the proposed triggered criteria are satisfied, thereby preventing the unnecessary resource wastage. Previously, a dynamic ETM [26] was proposed to tackle the energy consumption problem in the platooning control system. In Deng et al. [27], a novel periodic ETM based on a dynamic function was proposed to conserve network communication resources among subsystems, and a distributed observer was devised to remove the asynchronous behavior resulting from nonuniform transmission delays. In Zhu et al. [28], a type of event-triggered data-driven control scheme with quantization was studied. In Bai et al. [29], a gradient-based recursive reinforcement learning ETM was proposed to tackle the tracking problem in nonlinear MASs. This approach aimed to enhance the efficiency and effectiveness of MASs by utilizing event-based triggering and multiple gradient updating. In Xu et al. [30], a predefined time event-triggered control problem under a class of nonstrict feedback control structures was investigated, and a novel filter was designed to solve the complexity problem of the backstepping algorithm.

In addition, because of nonlinearities and uncertainties existing in various systems, system models are often complex and not easy to establish. Consequently, data-driven control has gained significant attention, and research in related fields has been conducted widely. For instance, model-free adaptive control (MFAC), as a representative data-driven control method, was first proposed by Hou and Xiong [31], and it only utilized input-output data from agents to design the controller without needing a system model. Additionally, the research on MFAC gave rise to the growth of data-driven iterative learning control (DDILC). Compared with traditional control methods, DDILC can effectively maintain a good control performance by capitalizing on the repetitive characteristics of the system. In Hui et al. [32], a class of DDILC method with an extended state observer was devised to solve the permanent magnet linear motor control problem. In Meng and Zhang [33], robust iterative learning control was investigated for a category of nonlinear time-varying systems characterized by nonrepetitive uncertainties.

Although many control methods are now available to ensure good system tracking performance, the control schemes notably often need to meet certain prescribed performance requirements in practical engineering applications, such as waverider vehicles [34–36], space target capturing manipulators [37], and dual-linear-motor-driven systems [38]. In response to this need, a control approach known as prescribed performance control (PPC) is proposed. The PPC algorithm guarantees that the tracking error remains within a predefined set. Furthermore, in previous studies [39, 40], a novel PPC scheme guaranteed a tracking error within a specified performance range in a specified settling time. However, the aforementioned literature based on system models may not apply to practical systems because of the complexity and unknown properties of models. Therefore, the data-driven PPC algorithm requires further investigation. Previously, Liu et al. [41] proposed a data-driven PPC algorithm for MASs, which ensured that the tracking error was maintained within a reasonably small range through the proper definition of a tracking error transformation. Furthermore, numerous physical systems exhibited repetitive characteristics, such as train systems [42] and robotic arms [43–45]. Consequently, iterative learning control (ILC) has gained widespread attention for its ability to guarantee good control performance through learning from repetitive characteristics. Currently, there are no PPC results in the field of ILC based on the data-driven method, particularly related results on conserving network communication resources.

Motivated by the preceding discussions, this article concentrates on the issue of the bipartite tracking control problem of MASs with the prescribed performance by using the dynamic event-triggered data-driven ILC (DET-DDILC) algorithm. Below are the main contributions of this article.

(1) Unlike the previous approach [46–48] that introduced a sliding surface to investigate the tracking performance of MASs after an unconstrained transformation, an improved iterative linear data model based on an unconstrained output signal is proposed, which reduces the complexity of the control scheme for MASs.

(2) Because of the introduction of unconstrained transformation, a novel dynamic event-triggered condition based on the time-iteration-varying function is established for the unconstrained output signal, which is operated considering the characteristics of the prescribed condition. Compared with a previous event-triggered mechanism [49–51], this approach is more practical.

This article is constructed as follows. Section 2 provides the problem formulation and presents the main results. Section 3 provides a detailed stability analysis of the designed DET-DDILC scheme. Section 4

presents a simulation case to illustrate the validity of the designed DET-DDILC algorithm. Finally, the conclusion of the article is given in Section 5.

2 Formulation of the problem and preliminary concepts

2.1 Preliminaries

The graph theory is introduced in this section. Specifically, $\mathcal{G} = (\mathcal{V}, \mathcal{E}, \mathcal{A})$ is a signed digraph, where $\mathcal{A} = [a_{ij}] \in \mathbb{R}^{N\times N}$ is the weighted adjacency matrix with the weights of -1, 0, and 1. The set of agents is represented by $\mathcal{V} = [v_1, v_2, \ldots, v_n]$, whereas the set of edges is given as $\mathcal{E} = \{(v_j, v_i)|v_i \in \mathcal{V}\} \subseteq \mathcal{V} \times \mathcal{V}$. Moreover, N_i denotes the set of neighbor agents of agent i, and V_1, V_2 are two sets of agents with the following properties: $V_1 \cup V_2 = \mathcal{V}, V_1 \cap V_2 = \emptyset$. Specifically, agents within the same subset exhibit cooperative relationships, whereas agents outside of the subsets exhibit competitive relationships. That is, if $(v_j, v_i) \in \mathcal{E}$ and $v_i, v_j \in V_1$, $a_{ij} = 1$, if $(v_j, v_i) \in \mathcal{E}$ and $v_i \in V_1, v_j \in V_2$, $a_{ij} = -1$, otherwise, $a_{ij} = 0$. Furthermore, the Laplacian matrix $\mathcal{L}$ of $\mathcal{G}$ is described as $\mathcal{L} = \mathcal{B} - \mathcal{A}$, where $\mathcal{B} = \text{diag}\{b_i\}_{i=1}^n$ with $b_i = \sum_{j\in N_i} |a_{ij}|$ being the in-degree vertex. Notably, $\mathcal{G}$ is strongly connected.

2.2 System modeling

Consider a group of N agents, where the dynamics of agent i is expressed as

$$y_i(\mathfrak{p}, \mathfrak{s}+1) = f_i(y_i(\mathfrak{p}, \mathfrak{s}), u_i(\mathfrak{p}, \mathfrak{s})), i \in \mathcal{V}, \tag{1}$$

where $f_i(\cdot)$ is an unknown function, and $\mathfrak{p} \in \{1, 2, \ldots\}$ and $\mathfrak{s} \in \{1, 2, \ldots, T\}$ are the number of iterations and time instants, respectively. $T \in Z^+$ is the terminal instant with Z^+ representing the positive integer. Additionally, $y_i(\mathfrak{p}, \mathfrak{s})$ and $u_i(\mathfrak{p}, \mathfrak{s})$ denote the system output and the control input of agent i, respectively.

This article uses the following assumptions and lemmas.

Assumption 1. The partial derivative of $f_i(\cdot)$ with respect to the control input $u_i(\mathfrak{p}, \mathfrak{s})$ is assumed to be continuous.

Assumption 2 ([12,13,18])**.** The ratio of $\Delta u_i(\mathfrak{p}, \mathfrak{s})$ and $\Delta u_j(\mathfrak{p}, \mathfrak{s})$ is bounded, that is, $|\Delta u_j(\mathfrak{p}, \mathfrak{s})/\Delta u_i(\mathfrak{p}, \mathfrak{s})| \leqslant \wp$, where $\wp$ is a positive constant.

Assumption 3. The signed graph $\mathcal{G}$ owns a directed spanning tree.

Assumption 4. System (1) adheres to the generalized Lipschitz condition, that is, if $|\Delta u_i(\mathfrak{p}, \mathfrak{s})| \neq 0$,

$$|\Delta y_i(\mathfrak{p}, \mathfrak{s}+1)| \leqslant b_1 |\Delta u_i(\mathfrak{p}, \mathfrak{s})|$$

holds, where $\Delta u_i(\mathfrak{p}, \mathfrak{s}) = u_i(\mathfrak{p}, \mathfrak{s}) - u_i(\mathfrak{p}-1, \mathfrak{s})$ and b_1 is a positive constant.

Assumption 5 ([52])**.** The sign of the pseudo partial derivative (PPD) parameter is unchanged and satisfies $\varphi_i(\mathfrak{p}, \mathfrak{s}) > o$ or $\varphi_i(\mathfrak{p}, \mathfrak{s}) < o$ with $o > 0$ being a positive constant for all $\mathfrak{p} \in \{1, 2, \ldots\}$ and $\mathfrak{s} \in \{1, 2, \ldots, T\}$. In general, it is assumed that $\varphi_i(\mathfrak{p}, \mathfrak{s}) > o$.

Remark 1. Assumption 1 represents a traditional constraint for designing a general nonlinear system. Assumption 2 is employed as a prerequisite for the demonstration of Lemma 2. Assumption 3 serves as both a necessary and sufficient condition to guarantee that the scheme can be accomplished. Assumption 4 presents a limit on the upper bound of the system output increments, which can be explained from an energy perspective, such as the platooning system [53], the helicopter system [54], and the train system [55]. Assumption 5 implies that the sign of the control input remains unchanged, which is also applicable to some model-based nonlinear systems.

Lemma 1 ([56–58])**.** For nonlinear MASs (1) satisfying Assumptions 1 and 4, when $|\Delta u_i(\mathfrak{p}, \mathfrak{s})| \neq 0$ holds, there exists a PPD parameter $\phi_i(\mathfrak{p}, \mathfrak{s})$ such that nonlinear MASs (1) can be converted into the below iterative compact format dynamic linearization (iCFDL) model:

$$\Delta y_i(\mathfrak{p}, \mathfrak{s}+1) = \phi_i(\mathfrak{p}, \mathfrak{s}) \Delta u_i(\mathfrak{p}, \mathfrak{s}), \tag{2}$$

where $\Delta y_i(\mathfrak{p}, \mathfrak{s}+1) = y_i(\mathfrak{p}, \mathfrak{s}+1) - y_i(\mathfrak{p}-1, \mathfrak{s}+1)$ and $|\phi_i(\mathfrak{p}, \mathfrak{s})| \leqslant b_1$.

Considering a bipartite tracking problem, the distributed bipartite measurement output of the ith agent is defined as

$$\xi_i(\mathfrak{p},\mathfrak{s}) = \sum_{j\in N_i} |a_{ij}|(\text{sign}(a_{ij})y_j(\mathfrak{p},\mathfrak{s}) - y_i(\mathfrak{p},\mathfrak{s})) + d_i(w_i y_d(\mathfrak{s}) - y_i(\mathfrak{p},\mathfrak{s})), \tag{3}$$

where sign$(\cdot)$ is the sign function. Additionally, if agent i can receive the reference signal from the leader, then $d_i = 1$; otherwise, $d_i = 0$. Furthermore, if agent $i \in V_1$, then $w_i = 1$, and if agent $i \in V_2$, then $w_i = -1$.

Taking (1) into (3), obviously, the bipartite output exhibits the form of a nonlinear function as below:

$$\xi_i(\mathfrak{p},\mathfrak{s}+1) = P_i[y_i(\mathfrak{p},\mathfrak{s}), u_i(\mathfrak{p},\mathfrak{s}), y_j(\mathfrak{p},\mathfrak{s}), u_j(\mathfrak{p},\mathfrak{s})], \tag{4}$$

where $P_i(\cdot), i = 1, 2, \ldots, N$ represents an unknown nonlinear function.

Consequently, an iCFDL model for MASs can be derived similar to Lemma 1 in [12, 18].

Lemma 2. If Eq. (4) satisfies Assumptions 1, 2, 4, and $|\Delta u_i(\mathfrak{p},\mathfrak{s})| \geqslant \jmath_i$ holds, where $\jmath_i > 0$ is a constant, then there exists a PPD parameter $\varphi_i^c(\mathfrak{p},\mathfrak{s})$ such that

$$\Delta\xi_i(\mathfrak{p},\mathfrak{s}+1) = \varphi_i^c(\mathfrak{p},\mathfrak{s})\Delta u_i(\mathfrak{p},\mathfrak{s}), \tag{5}$$

where $\Delta\xi_i(\mathfrak{p},\mathfrak{s}+1) = \xi_i(\mathfrak{p},\mathfrak{s}+1) - \xi_i(\mathfrak{p}-1,\mathfrak{s}+1)$ and $\varphi_i^c(\mathfrak{p},\mathfrak{s})$ satisfies $|\varphi_i^c(\mathfrak{p},\mathfrak{s})| \leqslant k_1$ with k_1 being a positive constant.

Proof. According to (4), $\Delta\xi_i(\mathfrak{p},\mathfrak{s}+1)$ can be deduced as follows:

$$\begin{aligned}\Delta\xi_i(\mathfrak{p},\mathfrak{s}+1) =\ & P_i[y_i(\mathfrak{p},\mathfrak{s}), u_i(\mathfrak{p},\mathfrak{s}), y_j(\mathfrak{p},\mathfrak{s}), u_j(\mathfrak{p},\mathfrak{s})]\\ & -P_i[y_i(\mathfrak{p},\mathfrak{s}), u_i(\mathfrak{p}-1,\mathfrak{s}), y_j(\mathfrak{p},\mathfrak{s}), u_j(\mathfrak{p},\mathfrak{s})]\\ & +P_i[y_i(\mathfrak{p},\mathfrak{s}), u_i(\mathfrak{p}-1,\mathfrak{s}), y_j(\mathfrak{p},\mathfrak{s}), u_j(\mathfrak{p},\mathfrak{s})]\\ & -P_i[y_i(\mathfrak{p}-1,\mathfrak{s}), u_i(\mathfrak{p}-1,\mathfrak{s}), y_j(\mathfrak{p}-1,\mathfrak{s}), u_j(\mathfrak{p}-1,\mathfrak{s})].\end{aligned} \tag{6}$$

Then, using the differential mean value theorem with respect to $u_i(\mathfrak{p},\mathfrak{s})$ for the first and second terms, we have

$$\Delta\xi_i(\mathfrak{p},\mathfrak{s}+1) = \frac{\partial P_i^*}{\partial u_i(\mathfrak{p},\mathfrak{s})}\Delta u_i(\mathfrak{p},\mathfrak{s}) + \Psi_i(\mathfrak{p},\mathfrak{s}), \tag{7}$$

where $\Psi_i(\mathfrak{p},\mathfrak{s}) = \eta_i(\mathfrak{p},\mathfrak{s})\Delta u_i(\mathfrak{p},\mathfrak{s}) + \eta_j(\mathfrak{p},\mathfrak{s})\Delta u_j(\mathfrak{p},\mathfrak{s})$; then combining with Assumption 2, we can find $\eta_i^*(\mathfrak{p},\mathfrak{s})$ such that $\Psi_i(\mathfrak{p},\mathfrak{s}) = \eta_i^*(\mathfrak{p},\mathfrak{s})\Delta u_i(\mathfrak{p},\mathfrak{s})$, namely, $\varphi_i^c(\mathfrak{p},\mathfrak{s}) = \frac{\partial P_i^*}{\partial u_i(\mathfrak{p},\mathfrak{s})} + \eta_i^*(\mathfrak{p},\mathfrak{s})$; then Eq. (5) can be obtained. Additionally, according to Assumptions 2, 4, 6 and $|\Delta u_i(\mathfrak{p},\mathfrak{s})| \geqslant \jmath_i$, one has

$$\begin{aligned}|\Delta\xi_i(\mathfrak{p},\mathfrak{s}+1)| &\leqslant \left|\sum_{j\in N_i} |a_{ij}|(a_{ij}b_1|\wp||\Delta u_i(\mathfrak{p},\mathfrak{s})| + b_1|\Delta u_i(\mathfrak{p},\mathfrak{s})|) + d_i(r_d + b_i|\Delta u_i(\mathfrak{p},\mathfrak{s})|)\right|\\ &\leqslant \big(N(1+|\wp|)b_1 + d_i b_1 + \bar{r}\big)|\Delta u_i(\mathfrak{p},\mathfrak{s})|\\ &\leqslant k_1|\Delta u_i(\mathfrak{p},\mathfrak{s})|,\end{aligned} \tag{8}$$

where $k_1 = (N(1+\wp)b_1 + d_i b_1 + \bar{r})$ with $\bar{r} = \frac{r_d}{\jmath_i}$, and from (5) and (8), we have $|\varphi_i^c(\mathfrak{p},\mathfrak{s})| < k_1$.

2.3 Prescribed performance function

To guarantee that the distributed bipartite measurement output $\xi_i(\mathfrak{p},\mathfrak{s})$ always converges to the predefined region, the following constraint condition is considered:

$$-\Gamma(\mathfrak{s}) < \xi_i(\mathfrak{p},\mathfrak{s}) < \Gamma(\mathfrak{s}), \tag{9}$$

and the prescribed function $\Gamma(s)$ is given as

$$\Gamma(\mathfrak{s}+1) = (1-z)\Gamma(\mathfrak{s}) + z\Gamma_\infty, \tag{10}$$

$$\lim_{\mathfrak{s}\to\infty}\Gamma(\mathfrak{s}) = \Gamma_\infty \tag{11}$$

with the initial value $\Gamma(0) > \Gamma_\infty > 0$ and $z \in (0,1)$ being the convergence rate of the prescribed function $\Gamma(\mathfrak{s})$.

Obviously, the constraint condition for $\xi_i(\mathfrak{p},\mathfrak{s})$ presented in (9) increases the complexity of the controller design. Therefore, firstly we need to transform the constrained bipartite measurement output $\xi_i(\mathfrak{p},\mathfrak{s})$ into an unconstrained one, the following transformation is constructed:

$$\xi_i(\mathfrak{p},\mathfrak{s}) = \Gamma(s)\mho\big(\tau_i(\mathfrak{p},\mathfrak{s})\big), \tag{12}$$

where $\tau_i(\mathfrak{p},\mathfrak{s})$ is the transformed output and $\mho\big(\tau_i(\mathfrak{p},\mathfrak{s})\big)$ is a strictly increasing function satisfying:

$$\mho\big(\tau_i(\mathfrak{p},\mathfrak{s})\big) \in (-1,1), \tag{13}$$

$$\lim_{\tau_i(\mathfrak{p},\mathfrak{s})\to\infty} \mho\big(\tau_i(\mathfrak{p},\mathfrak{s})\big) = 1,$$

$$\lim_{\tau_i(\mathfrak{p},\mathfrak{s})\to-\infty} \mho\big(\tau_i(\mathfrak{p},\mathfrak{s})\big) = -1. \tag{14}$$

Since $\mho\big(\tau_i(\mathfrak{p},\mathfrak{s})\big)$ is strictly increasing, therefore, $\mho(\cdot)$ can be selected as

$$\mho\big(\tau_i(\mathfrak{p},\mathfrak{s})\big) = \frac{\mathrm{e}^{\tau_i(\mathfrak{p},\mathfrak{s})} - \mathrm{e}^{-\tau_i(\mathfrak{p},\mathfrak{s})}}{\mathrm{e}^{\tau_i(\mathfrak{p},\mathfrak{s})} + \mathrm{e}^{-\tau_i(\mathfrak{p},\mathfrak{s})}}. \tag{15}$$

Then, the transformed output $\tau_i(\mathfrak{p},\mathfrak{s})$ is described as

$$\tau_i(\mathfrak{p},\mathfrak{s}) = \frac{1}{2}\ln\left(\frac{\Gamma(\mathfrak{s}) + \xi_i(\mathfrak{p},\mathfrak{s})}{\Gamma(\mathfrak{s}) - \xi_i(\mathfrak{p},\mathfrak{s})}\right). \tag{16}$$

Lemma 3. Since $\tau_i(\mathfrak{p},\mathfrak{s})$ is the transformed output generated by the distributed bipartite measurement output $\xi_i(\mathfrak{p},\mathfrak{s})$ via the homeomorphism mapping function, therefore, if Assumptions 1, 2, 4 and $|\Delta u_i(\mathfrak{p},\mathfrak{s})| \geqslant \jmath_i$ hold, there exists a PPD parameter $\varphi_i(\mathfrak{p},\mathfrak{s})$ such that the transformed output $\tau_i(\mathfrak{p},\mathfrak{s})$ can be expressed as the unconstrained iterative linear data model (UILDM) below:

$$\Delta\tau_i(\mathfrak{p},\mathfrak{s}+1) = \varphi_i(\mathfrak{p},\mathfrak{s})\Delta u_i(\mathfrak{p},\mathfrak{s}). \tag{17}$$

Similarly, $\varphi_i(\mathfrak{p},\mathfrak{s})$ satisfies $|\varphi_i(\mathfrak{p},\mathfrak{s})| \leqslant f_1$ with f_1 being a positive constant.

Proof. Because the prescribed function $\Gamma(\mathfrak{s})$ used to constrain the bipartite measurement output $\xi_i(\mathfrak{p},\mathfrak{s})$ is bounded and monotonically decreasing along the time axis, therefore, the proof concerning the homeomorphism transformed output $\tau_i(\mathfrak{p},\mathfrak{s})$ is similar to Lemma 2. Here is omitted.

Remark 2. The strictly increasing function $\mho(\cdot)$ is used to convert the distributed bipartite measurement output $\xi_i(\mathfrak{p},\mathfrak{s})$ into an unconstrained equivalent form $\tau_i(p,k)$. Consequently, considering the characteristics of the function $\mho(\tau_i(\mathfrak{p},\mathfrak{s}))$ mentioned in (13)–(15), one can infer that if $\tau_i(\mathfrak{p},\mathfrak{s})$ is bounded, then we can deduce $\xi_i(\mathfrak{p},\mathfrak{s})$ satisfies the constraint condition (9), namely, $-\Gamma(s) < \xi_i(\mathfrak{p},\mathfrak{s}) < \Gamma(s)$ holds.

2.4 Dynamic event-triggered data-driven ILC design

In practice, the true value of the PPD parameter $\varphi_i(\mathfrak{p},\mathfrak{s})$ is difficult to achieve. To address the problem, the following estimation law is utilized to update the PPD parameter estimator:

$$\hat{\varphi}_i(\mathfrak{p},\mathfrak{s}) = \hat{\varphi}_i(\mathfrak{p}-1,\mathfrak{s}) + \frac{\eta_i\Delta u_i(\mathfrak{p}-1,\mathfrak{s})}{\mu_i + \Delta u_i^2(\mathfrak{p}-1,\mathfrak{s})}[\Delta\tau_i(\mathfrak{p}-1,\mathfrak{s}+1) - \hat{\varphi}_i(\mathfrak{p}-1,\mathfrak{s})\Delta u_i(\mathfrak{p}-1,\mathfrak{s})], \tag{18}$$

where $0 < \eta_i < 1$ represents the step-size factor, while $\mu_i > 0$ denotes the penalty factor.

The following performance function is proposed for the controller design, namely:

$$J[u_i(\mathfrak{p},\mathfrak{s})] = |\tau_i(\mathfrak{p},\mathfrak{s}+1)|^2 + \lambda_i|u_i(\mathfrak{p},\mathfrak{s}) - u_i(\mathfrak{p}-1,\mathfrak{s})|^2. \tag{19}$$

Then, calculating the derivative of $J[u_i(\mathfrak{p},\mathfrak{s})]$ with respect to $u_i(\mathfrak{p},\mathfrak{s})$ and equating it to zero, the following update law of the controller is derived:

$$u_i(\mathfrak{p},\mathfrak{s}) = u_i(\mathfrak{p}-1,\mathfrak{s}) - \frac{\rho_i\hat{\varphi}_i(\mathfrak{p},\mathfrak{s})}{\lambda_i + \hat{\varphi}_i^2(\mathfrak{p},\mathfrak{s})}\tau_i(\mathfrak{p}-1,\mathfrak{s}+1), \tag{20}$$

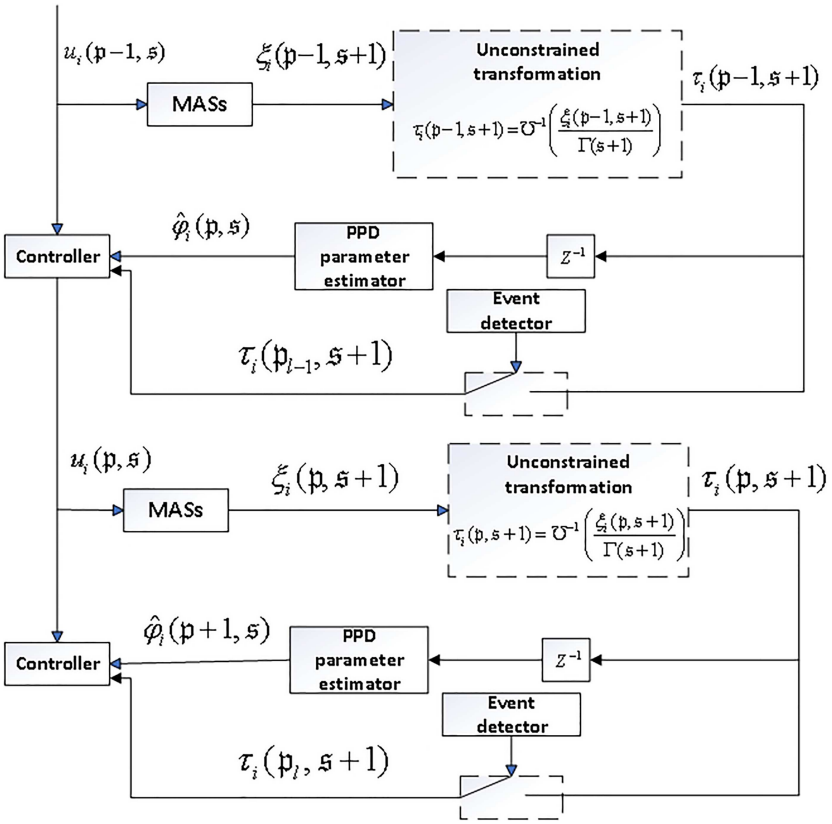

Figure 1 (Color online) System block diagram.

where the functions of ρ_i and λ_i are similar to η_i and μ_i, respectively.

Then, incorporating the event-triggered mechanism and setting the trigger error as $T_i(\mathfrak{p},\mathfrak{s}) = \tau_i(\mathfrak{p}_l,\mathfrak{s}) - \tau_i(\mathfrak{p},\mathfrak{s})$, where $\mathfrak{p}_l$ $(l = 1, 2, \ldots)$ is the event-triggered iterative sequence. Subsequently, the dynamic event-triggered function is devised as follows:

$$f_i(\mathfrak{p},\mathfrak{s}) = \frac{1}{v}|\gamma_i(\mathfrak{p},\mathfrak{s})| + w - |T_i(\mathfrak{p},\mathfrak{s})|, \tag{21}$$

where w and v are positive constants. And $\gamma_i(\mathfrak{p},\mathfrak{s})$ denotes the dynamic variable that satisfies the following conditions:

$$\gamma_i(\mathfrak{p}+1,\mathfrak{s}) = \chi\gamma_i(\mathfrak{p},\mathfrak{s}) + w - |T_i(\mathfrak{p},\mathfrak{s})|, \gamma_i(1,\mathfrak{s}) = \gamma_0, \tag{22}$$

where $\chi > 0$ is a parameter to be determined, and γ_0 is the initial value.

Therefore, the transformed output $\tau_i(\mathfrak{p},\mathfrak{s})$ will be transmitted once the following condition is satisfied:

$$\mathfrak{p}_{l+1} = \inf\{\mathfrak{p} \in \mathbb{N} \mid \mathfrak{p} > \mathfrak{p}_l, f_i(\mathfrak{p},\mathfrak{s}) < 0\}. \tag{23}$$

In conjunction with (20) and (23), when $\mathfrak{p} - 1 \in (\mathfrak{p}_{l-2}, \mathfrak{p}_{l-1}]$, the control input will be updated based on the following equation:

$$u_i(\mathfrak{p},\mathfrak{s}) = \begin{cases} u_i(\mathfrak{p}-1,\mathfrak{s}), & \mathfrak{p}-1 \in (\mathfrak{p}_{l-2},\mathfrak{p}_{l-1}), \\ u_i(\mathfrak{p}-1,\mathfrak{s}) - \frac{\rho_i\hat{\varphi}_i(\mathfrak{p},\mathfrak{s})}{\lambda_i+\hat{\varphi}_i^2(\mathfrak{p},\mathfrak{s})}\tau_i(\mathfrak{p}_{l-1},\mathfrak{s}+1), & \mathfrak{p}-1 = \mathfrak{p}_{l-1}. \end{cases} \tag{24}$$

From above descriptions and Figure 1, the distributed event-triggered data-driven iterative learning control (DET-DDILC) algorithm with the prescribed performance is established as below:

$$\hat{\varphi}_i(\mathfrak{p},\mathfrak{s}) = \hat{\varphi}_i(\mathfrak{p}-1,\mathfrak{s}) + \frac{\eta\Delta u_i(\mathfrak{p}-1,\mathfrak{s})}{\mu+\Delta u_i^2(\mathfrak{p}-1,\mathfrak{s})}[\Delta\tau_i(\mathfrak{p}-1,\mathfrak{s}+1) - \hat{\varphi}_i(\mathfrak{p}-1,\mathfrak{s})\Delta u_i(\mathfrak{p}-1,\mathfrak{s})], \tag{25}$$

$$\hat{\varphi}_i(\mathfrak{p},\mathfrak{s})=\hat{\varphi}_i(1,\mathfrak{s}),\ \text{if}\ |\hat{\varphi}_i(\mathfrak{p},\mathfrak{s})|\leqslant \jmath\ \text{or}\ |\Delta u_i(\mathfrak{p}-1,\mathfrak{s})|\leqslant \jmath\ \text{or}\ \text{sign}(\hat{\varphi}_i(\mathfrak{p},\mathfrak{s}))\neq \text{sign}(\hat{\varphi}_i(1,\mathfrak{s})), \tag{26}$$

$$u_i(\mathfrak{p},\mathfrak{s})=\begin{cases} u_i(\mathfrak{p}-1,\mathfrak{s}), & \mathfrak{p}-1\in(\mathfrak{p}_{l-2},\mathfrak{p}_{l-1}),\\ u_i(\mathfrak{p}-1,\mathfrak{s})-\frac{\rho_i\hat{\varphi}_i(\mathfrak{p},\mathfrak{s})}{\lambda_i+\hat{\varphi}_i^2(\mathfrak{p},\mathfrak{s})}\tau_i(\mathfrak{p}_{l-1},\mathfrak{s}+1), & \mathfrak{p}-1=\mathfrak{p}_{l-1}, \end{cases} \tag{27}$$

where $\jmath>0$ represents a very small positive parameter.

Remark 3. The resetting algorithm (26) is used to prevent the PPD parameter estimated law (25) from not updating, and to ensure that the PPD parameter estimated law (25) can track the iteration-varying parameters well.

Problem 1. For MASs (1), the objective is to design a prescribed performance DET-DDILC scheme composed by (25)–(27) to ensure that the transformed output $\tau_i(\mathfrak{p},\mathfrak{s})$ is uniformly ultimately bounded. Namely,

$$\left\{\tau_i(\mathfrak{p},\mathfrak{s})\Big|\lim_{\mathfrak{p}\to\infty}|\tau_i(\mathfrak{p},\mathfrak{s})|\leqslant b_\tau\right\} \tag{28}$$

with b_τ being a positive constant.

3 Stability analysis

The stability analysis of MASs (1) is presented by proving that the transformed output $\tau_i(\mathfrak{p},\mathfrak{s})$ is uniformly ultimately bounded in this section.

Theorem 1. For MASs (1), Problem 1 can be solved by using the DET-DDILC algorithm (25)–(27), if there exists $\lambda_i>\lambda_{\min}$ with $\lambda_{\min}>0$, $\rho_i\in(0,1]$, $\mu_i>0$, $\eta_i\in(0,1]$, $w>0$, $\chi>0$, $v>0$ such that the following condition holds:

$$0<\chi+\frac{1}{v}<1. \tag{29}$$

Proof. The proof is divided into two main parts, including the boundness of $\varphi_i(\mathfrak{p},\mathfrak{s})$ and the boundness of the transformed output $\tau_i(\mathfrak{p},\mathfrak{s})$.

Part I: The boundness of $\varphi_i(\mathfrak{p},\mathfrak{s})$. Define the PPD parameter estimation error as $\widetilde{\varphi}_i(\mathfrak{p},\mathfrak{s})=\hat{\varphi}_i(\mathfrak{p},\mathfrak{s})-\varphi_i(\mathfrak{p},\mathfrak{s})$. Then, subtracting $\varphi_i(\mathfrak{p},\mathfrak{s})$ from both sides of (25) yields

$$\begin{aligned}\widetilde{\varphi}_i(\mathfrak{p},\mathfrak{s})&=\widetilde{\varphi}_i(\mathfrak{p}-1,\mathfrak{s})-\Delta\varphi_i(\mathfrak{p},\mathfrak{s})+\frac{\eta_i\big(\Delta\tau_i(\mathfrak{p}-1,\mathfrak{s}+1)-\hat{\varphi}_i(\mathfrak{p}-1,\mathfrak{s})\Delta u_i(\mathfrak{p}-1,\mathfrak{s})\big)}{\mu_i+|\Delta u_i(\mathfrak{p}-1,\mathfrak{s})|^2}\\&=\left(1-\frac{\eta_i\Delta u_i^2(\mathfrak{p}-1,\mathfrak{s})}{\mu_i+|\Delta u_i(\mathfrak{p}-1,\mathfrak{s})|^2}\right)\widetilde{\varphi}_i(\mathfrak{p}-1,\mathfrak{s})-\Delta\varphi_i(\mathfrak{p},\mathfrak{s}).\end{aligned} \tag{30}$$

By selecting $0<\eta_i<1$ and $\mu_i>0$, we have

$$0<\left|1-\frac{\eta_i\Delta u_i^2(\mathfrak{p}-1,\mathfrak{s})}{\mu_i+|\Delta u_i(\mathfrak{p}-1,\mathfrak{s})|^2}\right|\leqslant d_1<1, \tag{31}$$

where d_1 is a positive constant.

Then, taking the absolute values on both sides of (31) yields

$$\begin{aligned}|\widetilde{\varphi}_i(\mathfrak{p},\mathfrak{s})|&\leqslant d_1|\widetilde{\varphi}_i(\mathfrak{p}-1,\mathfrak{s})|+2f_1\\&\ \ \vdots\\&\leqslant d_1^{\mathfrak{p}-1}|\widetilde{\varphi}_i(1,\mathfrak{s})|+\frac{2f_1(1-d_1^{\mathfrak{p}-1})}{1-d_1}.\end{aligned} \tag{32}$$

The statement above implies that $\widetilde{\varphi}_i(\mathfrak{p},\mathfrak{s})$ is uniformly bounded, which consequently deduces the conclusion that $\hat{\varphi}_i(\mathfrak{p},\mathfrak{s})$ is also bounded because of the boundedness of $\varphi_i(\mathfrak{p},\mathfrak{s})$.

Part II: The boundness of $\tau_i(\mathfrak{p},\mathfrak{s})$. For the convenience of subsequent proofs, the boundedness of $\gamma_i(\mathfrak{p},\mathfrak{s})$ needs to be proven first.

From the dynamic event-triggered condition in (23), one can deduce $\frac{1}{v}|\gamma_i(\mathfrak{p},\mathfrak{s})| + w - |T_i(\mathfrak{p},\mathfrak{s})| \geqslant 0$. Consequently, the dynamical variable specified in (22) satisfies

$$\begin{aligned}
|\gamma_i(\mathfrak{p}+1,\mathfrak{s})| &\leqslant \chi|\gamma_i(\mathfrak{p},\mathfrak{s})| + w + |T_i(\mathfrak{p},\mathfrak{s})| \\
&\leqslant \chi|\gamma_i(\mathfrak{p},\mathfrak{s})| + w + \frac{1}{v}|\gamma_i(\mathfrak{p},\mathfrak{s})| + w \\
&\leqslant \left(\chi + \frac{1}{v}\right)|\gamma_i(\mathfrak{p},\mathfrak{s})| + 2w \\
&\leqslant \left(\chi + \frac{1}{v}\right)^2 |\gamma_i(\mathfrak{p}-1,\mathfrak{s})| + 2w\left(\chi + \frac{1}{v}\right) + 2w \\
&\vdots \\
&\leqslant \left(\chi + \frac{1}{v}\right)^{\mathfrak{p}} |\gamma_i(1,\mathfrak{s})| + \frac{2w[1-(\chi+\frac{1}{v})^{\mathfrak{p}}]}{1-(\chi+\frac{1}{v})}.
\end{aligned} \tag{33}$$

Then, based on (29), $\gamma_i(\mathfrak{p},\mathfrak{s})$ converges to the set below:

$$\left\{\gamma_i(\mathfrak{p},\mathfrak{s}) \middle| \lim_{\mathfrak{p}\to\infty} |\gamma_i(\mathfrak{p},\mathfrak{s})| \leqslant \frac{2\omega}{1-\left(\chi+\frac{1}{\nu}\right)}\right\}. \tag{34}$$

Namely, $\gamma_i(\mathfrak{p},\mathfrak{s})$ is uniformly bounded.

In addition, due to $T_i(\mathfrak{p}-1,\mathfrak{s}) = \tau_i(\mathfrak{p}_{l-1},\mathfrak{s}) - \tau_i(\mathfrak{p}-1,\mathfrak{s})$, taking (27) into (17), one can get

$$\begin{aligned}
\tau_i(\mathfrak{p},\mathfrak{s}+1) &= \tau_i(\mathfrak{p}-1,\mathfrak{s}+1) - \varphi_i(\mathfrak{p},\mathfrak{s})\frac{\rho_i\hat{\varphi}_i(\mathfrak{p},\mathfrak{s})}{\lambda_i+\hat{\varphi}_i^2(\mathfrak{p},\mathfrak{s})}\tau_i(\mathfrak{p}_{l-1},\mathfrak{s}+1) \\
&= \tau_i(\mathfrak{p}-1,\mathfrak{s}+1) - \varphi_i(\mathfrak{p},\mathfrak{s})\frac{\rho_i\hat{\varphi}_i(\mathfrak{p},\mathfrak{s})}{\lambda_i+\hat{\varphi}_i^2(\mathfrak{p},\mathfrak{s})}(\tau_i(\mathfrak{p}-1,\mathfrak{s}) + T_i(\mathfrak{p}-1,\mathfrak{s})) \\
&= \left(1 - \frac{\rho_i\varphi_i(\mathfrak{p},\mathfrak{s})\hat{\varphi}_i(\mathfrak{p},\mathfrak{s})}{\lambda_i+\hat{\varphi}_i^2(\mathfrak{p},\mathfrak{s})}\right)\tau_i(\mathfrak{p}-1,\mathfrak{s}) - \frac{\rho_i\varphi_i(\mathfrak{p},\mathfrak{s})\hat{\varphi}_i(\mathfrak{p},\mathfrak{s})}{\lambda_i+\hat{\varphi}_i^2(\mathfrak{p},\mathfrak{s})}T_i(\mathfrak{p}-1,\mathfrak{s}).
\end{aligned} \tag{35}$$

Then, taking the absolute value on both sides of (35), and bringing (21) into the following inequality, one can get

$$|\tau_i(\mathfrak{p},\mathfrak{s}+1)| \leqslant \left|1 - \frac{\rho_i\varphi_i(\mathfrak{p},\mathfrak{s})\hat{\varphi}_i(\mathfrak{p},\mathfrak{s})}{\lambda_i+\hat{\varphi}_i^2(\mathfrak{p},\mathfrak{s})}\right||\tau_i(\mathfrak{p}-1,\mathfrak{s})| + \frac{\rho_i\varphi_i(\mathfrak{p},\mathfrak{s})\hat{\varphi}_i(\mathfrak{p},\mathfrak{s})}{\lambda_i+\hat{\varphi}_i^2(\mathfrak{p},\mathfrak{s})}\left(\frac{1}{v}|\gamma_i(\mathfrak{p}-1,\mathfrak{s})| + w\right). \tag{36}$$

Then, letting $\lambda_{i,\min} = \frac{f_1^2}{4}$, there exists a constant $M_1 \in (0,1)$, which makes the inequality hold as follows:

$$0 < M_1 \leqslant \left|\frac{\varphi_i(\mathfrak{p},\mathfrak{s})\hat{\varphi}_i(\mathfrak{p},\mathfrak{s})}{\lambda_i+\hat{\varphi}_i^2(\mathfrak{p},\mathfrak{s})}\right| \leqslant \frac{f_1}{2\sqrt{\lambda_{i,\min}}} = 1. \tag{37}$$

Then, according to (37), $\rho_i \in (0,1]$, and $\lambda > \lambda_{i,\min}$, one has

$$\left|1 - \frac{\rho_i\varphi_i(\mathfrak{p},\mathfrak{s})\hat{\varphi}_i(\mathfrak{p},\mathfrak{s})}{\lambda_i+\hat{\varphi}_i^2(\mathfrak{p},\mathfrak{s})}\right| \leqslant 1 - \rho_i M_1 \triangleq d_2 < 1. \tag{38}$$

In addition, selecting appropriate values for v and w, and combining with (34), it is easy to get $|\frac{1}{v}|\gamma_i(\mathfrak{p}-1,\mathfrak{s})| + w| \leqslant b_\Omega$ with $b_\Omega > 0$ being the positive constant.

Then, combining with (36) and (38), one can deduce

$$\begin{aligned}
|\tau_i(\mathfrak{p},\mathfrak{s}+1)| &\leqslant d_2|\tau_i(\mathfrak{p}-1,\mathfrak{s}+1)| + b_\Omega \\
&\leqslant d_2^2|\tau_i(\mathfrak{p}-2,\mathfrak{s}+1)| + d_2 b_\Omega + b_\Omega \\
&\vdots
\end{aligned}$$

$$\leqslant d_2^{\mathfrak{p}-1}|\tau_i(1,\mathfrak{s}+1)| + \frac{b_\Omega(1-d_2^{\mathfrak{p}-1})}{1-d_2}. \tag{39}$$

This implies that $\tau_i(\mathfrak{p},\mathfrak{s})$ monotonically converges to the following set:

$$\left\{\tau_i(\mathfrak{p},\mathfrak{s})\Big|\lim_{\mathfrak{p}\to\infty}|\tau_i(\mathfrak{p},\mathfrak{s})| \leqslant \frac{b_\Omega}{1-d_2}\right\}. \tag{40}$$

Therefore, $\tau_i(\mathfrak{p},\mathfrak{s})$ is ultimately uniformly bounded, which implies that $\xi_i(\mathfrak{p},\mathfrak{s})$ satisfies the prescribed condition (9). In addition, when $\mathfrak{p} \in (\mathfrak{p}_{l-2},\mathfrak{p}_{l-1})$, i.e., the controller keeps the input data from the previous iteration, therefore it can be deduced that the transformed error $\tau_i(\mathfrak{p},\mathfrak{s})$ still converges. So far, the proof is completed.

Remark 4. By applying the principle of homeomorphism mapping, this paper converts the constrained measurement output $\xi_i(\mathfrak{p},\mathfrak{s})$ into an unconstrained one. In addition, in contrast to [41,46,47], a UILDM based on the transformed output $\tau_i(\mathfrak{p},\mathfrak{s})$ is designed in our work, which significantly reduces the complexity of the controller design.

4 Simulation example

Consider a group of MASs with the following dynamics:

$$\begin{aligned}
y_1(\mathfrak{p},\mathfrak{s}+1) &= 2u_1(\mathfrak{p},\mathfrak{s}) + \frac{y_1(\mathfrak{p},\mathfrak{s})u_1(\mathfrak{p},\mathfrak{s})}{1+y_1^2(\mathfrak{p},\mathfrak{s})},\\
y_2(\mathfrak{p},\mathfrak{s}+1) &= 2u_2(\mathfrak{p},\mathfrak{s}) + \frac{y_2(\mathfrak{p},\mathfrak{s})u_2(\mathfrak{p},\mathfrak{s})}{1+y_2^3(\mathfrak{p},\mathfrak{s})},\\
y_3(\mathfrak{p},\mathfrak{s}+1) &= 2u_3(\mathfrak{p},\mathfrak{s}) + \frac{y_3(\mathfrak{p},\mathfrak{s})u_3(\mathfrak{p},\mathfrak{s})}{1+y_3^4(\mathfrak{p},\mathfrak{s})},\\
y_4(\mathfrak{p},\mathfrak{s}+1) &= 2u_4(\mathfrak{p},\mathfrak{s}) + \frac{y_4(\mathfrak{p},\mathfrak{s})u_4(\mathfrak{p},\mathfrak{s})}{1+y_4^5(\mathfrak{p},\mathfrak{s})},\\
y_5(\mathfrak{p},\mathfrak{s}+1) &= 2u_5(\mathfrak{p},\mathfrak{s}) + \frac{y_5(\mathfrak{p},\mathfrak{s})u_5(\mathfrak{p},\mathfrak{s})}{1+y_5^6(\mathfrak{p},\mathfrak{s})},\\
y_6(\mathfrak{p},\mathfrak{s}+1) &= 2u_6(\mathfrak{p},\mathfrak{s}) + \frac{y_6(\mathfrak{p},\mathfrak{s})u_6(\mathfrak{p},\mathfrak{s})}{1+y_6^7(\mathfrak{p},\mathfrak{s})},\\
y_7(\mathfrak{p},\mathfrak{s}+1) &= 2u_7(\mathfrak{p},\mathfrak{s}) + \frac{y_7(\mathfrak{p},\mathfrak{s})u_7(\mathfrak{p},\mathfrak{s})}{1+y_7^8(\mathfrak{p},\mathfrak{s})}.
\end{aligned} \tag{41}$$

Figure 2 depicts a signed graph $\mathcal{G}$ exhibiting structural balance. In addition, the graph $\mathcal{G}$ consists of two subsets $V_1 = \{1,2,3,4\}$ and $V_2 = \{5,6,7\}$.

The Laplacian matrix of the graph $\mathcal{G}$ is given as

$$\mathcal{L} = \begin{bmatrix}
2 & 0 & -1 & -1 & 0 & 0 & 0\\
-1 & 1 & 0 & 0 & 0 & 0 & 0\\
0 & 0 & 2 & -1 & 0 & 1 & 0\\
-1 & -1 & 0 & 3 & 0 & 1 & 0\\
0 & 0 & 0 & 0 & 1 & -1 & 0\\
0 & 0 & 1 & 1 & 0 & 3 & -1\\
0 & 0 & 0 & 0 & -1 & -1 & 2
\end{bmatrix}, \tag{42}$$

and $\mathcal{D} = \mathrm{diag}\{1,0,1,0,1,0,1\}$.

Furthermore, the desired signal given by the virtual leader 0 is with the following dynamics:

$$y_d(\mathfrak{s}) = \begin{cases} 0.3, & 0 < \mathfrak{s} < 700,\\ 0.5\sin(\frac{\pi\mathfrak{s}}{250}), & 700 \leqslant \mathfrak{s} \leqslant 1200. \end{cases} \tag{43}$$

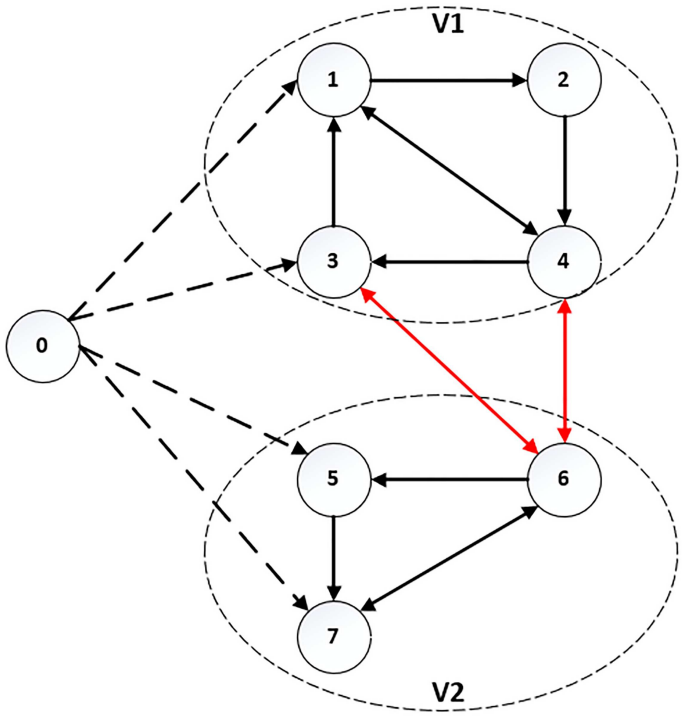

Figure 2 (Color online) Communication topology $\mathcal{G}$. The black lines show the partnership and the red lines indicate competitive ones.

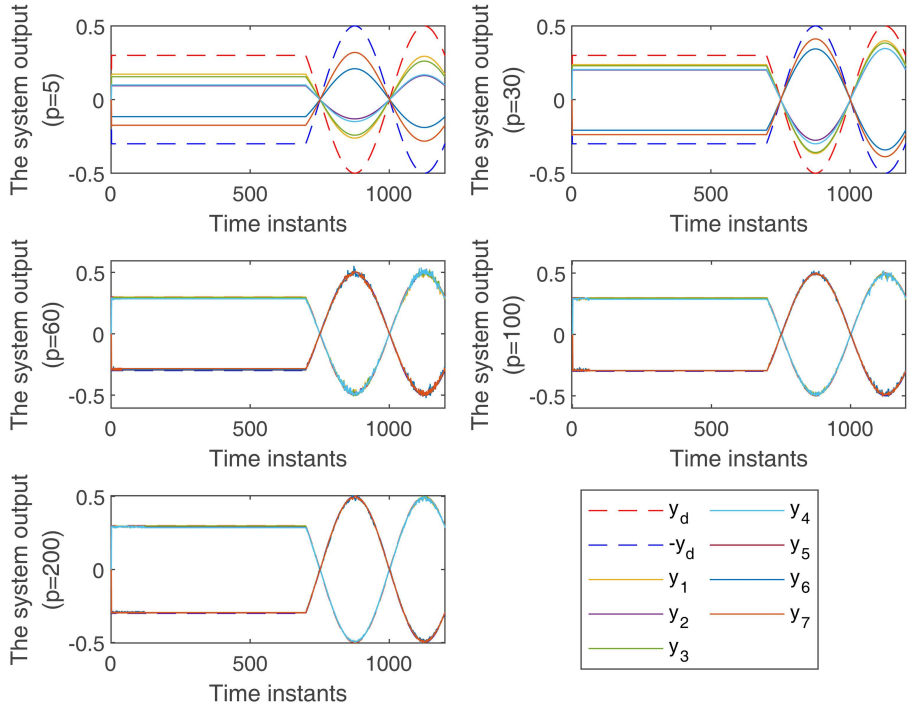

Figure 3 (Color online) System output with different iterations.

The initial conditions are chosen as $u_n(\mathfrak{p},1)=0$, $y_n(\mathfrak{p},1)=0$, where $\mathfrak{p}\in\{1,2,\ldots\}$ and $n\in\{1,2,\ldots,7\}$. For the first iteration, the initial values are selected as $u_n(1,\mathfrak{s})=0$, $\varphi_n(1,\mathfrak{s})=3.6$, and $\Gamma(1)=1.5$. The control parameters are selected as $\rho_n=0.6$, $\lambda_n=0.6$, $\eta_n=0.4$, $\mu_n=1$, $z=0.7$, and $\Gamma_\infty=0.065$. In addition, the trigger parameters and the initial value of the time-iteration-varying function are selected as $v=20$, $\chi=0.5$, $w=0.02$, and $\gamma_0=1$, respectively.

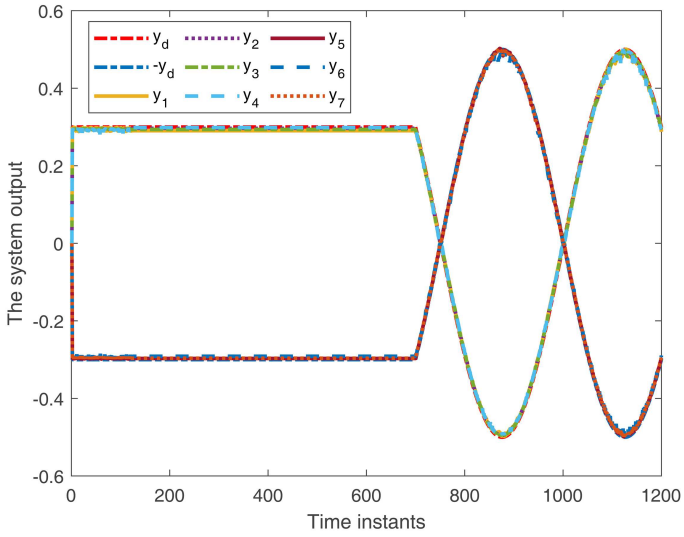

Figure 4 (Color online) Tracking performance at the 200th iteration.

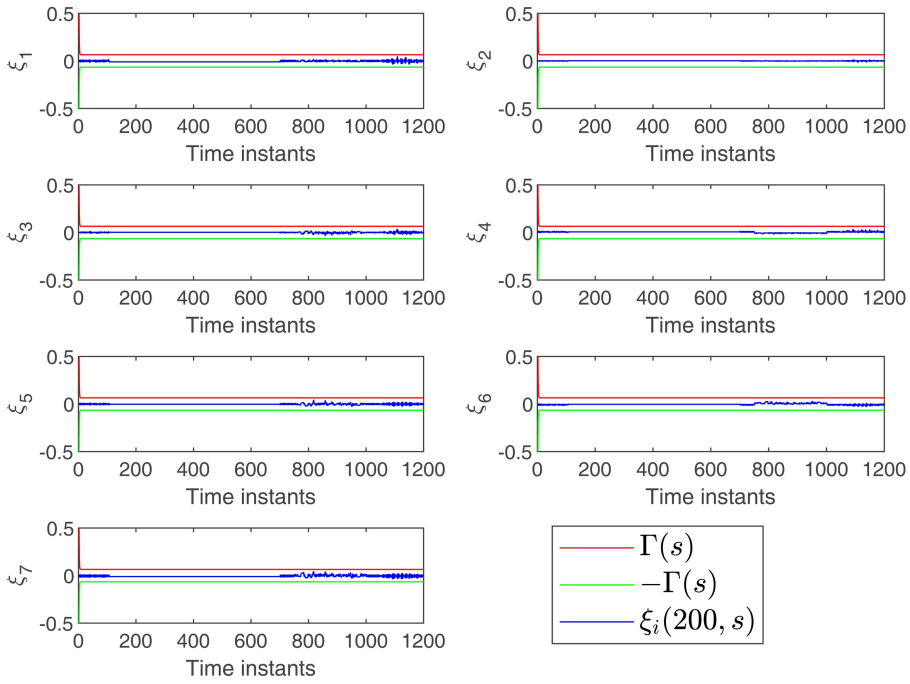

Figure 5 (Color online) Bipartite measurement output with prescribed performance at the 200th iteration.

Figure 3 illustrates the system outputs at the 5th, 30th, 60th, 100th, and 200th iterations. As depicted in Figure 3, the system performance improved as the number of iterations increased, demonstrating the effectiveness of the designed DET-DDILC scheme. Figure 4 indicates that the tracking performance of seven agents can be guaranteed at the 200th iteration by the proposed DET-DDILC control scheme. In addition, Figure 5 shows the bipartite measurement output with the prescribed performance of seven agents. Apparently, the bipartite measurement output $\xi_n(200, \mathfrak{s})$ was within the preset range under the proposed DET-DDILC control scheme.

In addition, for comparison with existing work [56], the simulation was conducted by selecting one agent from each of the two competitive sets. Figure 6 displays the tracking performance of agents 3 and 5, with and without the consideration of the prescribed performance. Figure 6 shows that compared with that of a previous study [56], the tracking performance was better under the prescribed performance.

Furthermore, Figure 7 showcases the event-triggered frequency of the seven agents along the iteration

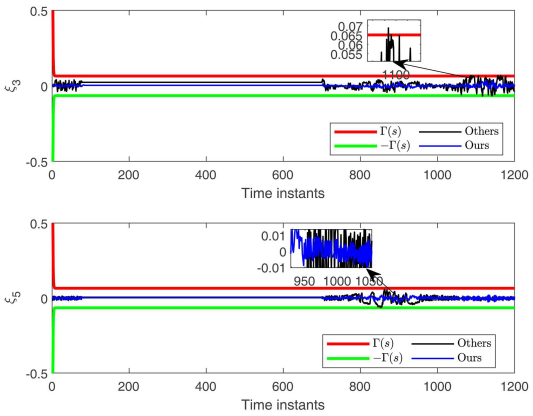

Figure 6 (Color online) Tracking performance at the 200th iteration compared with [56].

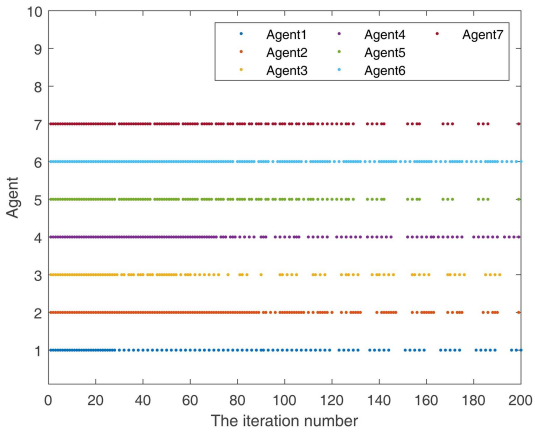

Figure 7 (Color online) Event-triggered frequency at the sampling instant $\mathfrak{s} = 900$.

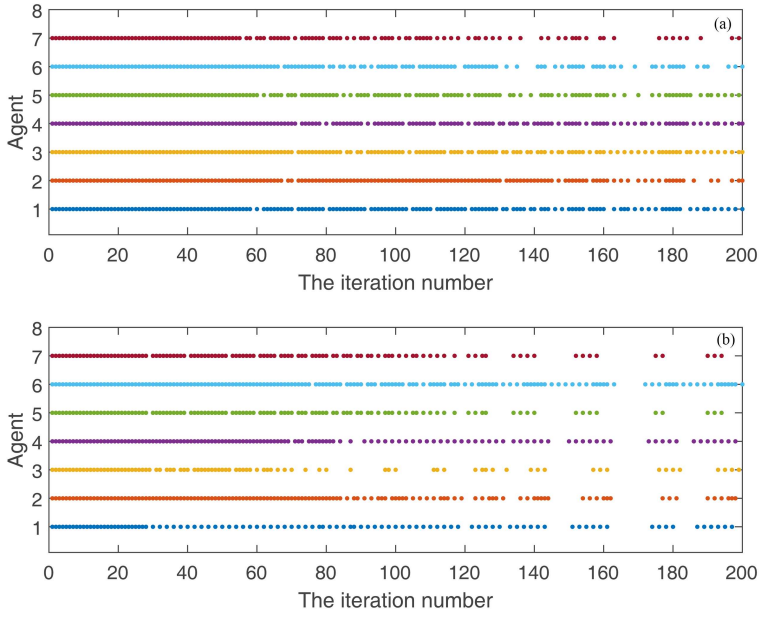

Figure 8 (Color online) Trigger frequency comparison. (a) Static event-triggered mechanism [59]; (b) ours.

axis at the 900th sampling instant. Notably, as the number of iterations increased, the event-triggered mechanism was triggered less frequently while maintaining excellent tracking performance. This demonstrated the effectiveness of the proposed event-triggered mechanism. In addition, Figure 8 compares the trigger frequency of the static event-triggered mechanism in a previous study [59] with the event-triggered mechanism designed in this study. The numbers of triggers for agent 3 are 159 using the static event-triggered mechanism [59] and 98 using our dynamic event-triggered mechanism. It demonstrates that the event-triggered mechanism we designed triggers fewer times for the same number of iterations.

5 Conclusion

In this study, the DET-DDILC algorithm with the prescribed performance was proposed to address the bipartite tracking problem subject to unknown heterogeneous MASs under signed graphs. By considering the prescribed performance, the distributed output was constrained within a selected strictly monotonically decreasing time-varying function. To convert the constrained distributed output into an unconstrained one, a strictly monotonically increasing function was designed. Furthermore, a dynamic event-triggered mechanism based on the time-iteration-varying function was used to conserve communica-

tion resources. In summary, the simulation result confirmed the effectiveness of the proposed DET-DDILC scheme.

Acknowledgements This work was supported by National Natural Science Foundation of China (Grant Nos. U1966202, 61873338, 62273191, 62233015), Taishan Scholars (Grant No. tsqn201812052), and Natural Science Foundation of Shandong Province (Grant No. ZR2020KF034).

References

1 Fax J A, Murray R M. Information flow and cooperative control of vehicle formations. IEEE Trans Automat Contr, 2004, 49: 1465–1476
2 Dong X, Hua Y, Zhou Y, et al. Theory and experiment on formation-containment control of multiple multirotor unmanned aerial vehicle systems. IEEE Trans Automat Sci Eng, 2019, 16: 229–240
3 Zhang D, Feng G, Shi Y, et al. Physical safety and cyber security analysis of multi-agent systems: a survey of recent advances. IEEE CAA J Autom Sin, 2021, 8: 319–333
4 Zhang L, Che W W, Deng C, et al. Prescribed performance control for multiagent systems via fuzzy adaptive event-triggered strategy. IEEE Trans Fuzzy Syst, 2022, 30: 5078–5090
5 Zhang S Q, Che W W, Deng C. Observer-based event-triggered control for linear MASs under a directed graph and DoS attacks. J Control Decision, 2022, 9: 384–396
6 Deng C, Zhang D, Feng G. Resilient practical cooperative output regulation for MASs with unknown switching exosystem dynamics under DoS attacks. Automatica, 2022, 139: 110172
7 Guo G, Kang J, Li R, et al. Distributed model reference adaptive optimization of disturbed multiagent systems with intermittent communications. IEEE Trans Cybern, 2022, 52: 5464–5473
8 Wang C, Zhang H, Zhang S. Cooperative output feedback consensus control of second-order nonlinear multi-agent systems under Markovian switching topologies. J Control Decision, 2023, 10: 476–483
9 Lu A Y, Yang G H. Distributed secure state estimation for linear systems against malicious agents through sorting and filtering. Automatica, 2023, 151: 110927
10 Chu C, Yuan Z, Hu S, et al. A pair-approximation method for modelling the dynamics of multi-agent stochastic games. In: Proceedings of the AAAI Conference on Artificial Intelligence, 2023. 37: 5565–5572
11 Liu J Z, Fan C Y, Peng Y C, et al. Emergent leader-follower relationship in networked multiagent systems. Sci China Inf Sci, 2023, 66: 229201
12 Ma Y S, Che W W, Deng C, et al. Distributed model-free adaptive control for learning nonlinear MASs under DoS attacks. IEEE Trans Neural Netw Learn Syst, 2023, 34: 1146–1155
13 Li F, Hou Z. Distributed model-free adaptive control for MIMO nonlinear multiagent systems under deception attacks. IEEE Trans Syst Man Cybern Syst, 2023, 53: 2281–2291
14 Ru X F, Mei C Y, Xia W G, et al. Distributed model-free adaptive predictive control of traffic lights for multiple interconnected intersections. Sci China Inf Sci, 2023, 66: 190209
15 Xu Y, Wu Z-G, Che W-W, et al. Reinforcement learning-based unknown reference tracking control of HMASs with nonidentical communication delays. Sci China Inf Sci, 2023, 66: 170203
16 Wang Z, Mu C, Hu S, et al. Modelling the dynamics of regret minimization in large agent populations: a master equation approach. In: Proceedings of the 31st International Joint Conference on Artificial Intelligence, Vienna, 2022. 23–29
17 Hu S, Leung C, Leung H. Modelling the dynamics of multiagent Q-learning in repeated symmetric games: a mean field theoretic approach. In: Proceedings of Advances in Neural Information Processing Systems, 2019. 32
18 Zhao H, Yu H, Peng L. Event-triggered distributed data-driven iterative learning bipartite formation control for unknown nonlinear multiagent systems. IEEE Trans Neural Netw Learn Syst, 2024, 35: 417–427
19 Hui Y, Chi R, Huang B, et al. Data-driven adaptive iterative learning bipartite consensus for heterogeneous nonlinear cooperation-antagonism networks. IEEE Trans Neural Netw Learn Syst, 2023, 34: 8262–8270
20 He W, Yu M, Yang T. Bipartite consensus of higher-order multi-agent systems based on event-triggered control and signed network. J Control Decision, 2021, 8: 233–242
21 Santos F C, Pacheco J M, Lenaerts T. Evolutionary dynamics of social dilemmas in structured heterogeneous populations. Proc Natl Acad Sci USA, 2006, 103: 3490–3494
22 Hauser O P, Hilbe C, Chatterjee K, et al. Social dilemmas among unequals. Nature, 2019, 572: 524–527
23 Wang Z, Jusup M, Wang R W, et al. Onymity promotes cooperation in social dilemma experiments. Sci Adv, 2017, 3: e1601444
24 Li X, Jusup M, Wang Z, et al. Punishment diminishes the benefits of network reciprocity in social dilemma experiments. Proc Natl Acad Sci USA, 2018, 115: 30–35
25 Wang Z, Jusup M, Shi L, et al. Exploiting a cognitive bias promotes cooperation in social dilemma experiments. Nat Commun, 2018, 9: 2954
26 Yue B F, Che W W. Data-driven dynamic event-triggered fault-tolerant platooning control. IEEE Trans Ind Inf, 2023, 19: 8418–8426
27 Deng C, Che W W, Wu Z G. A dynamic periodic event-triggered approach to consensus of heterogeneous linear multiagent systems with time-varying communication delays. IEEE Trans Cybern, 2021, 51: 1812–1821
28 Zhu P, Jin S, Bu X, et al. Improved model-free adaptive control for MIMO nonlinear systems with event-triggered transmission scheme and quantization. IEEE Trans Cybern, 2023, 53: 5867–5880
29 Bai W, Li T, Long Y, et al. Event-triggered multigradient recursive reinforcement learning tracking control for multiagent systems. IEEE Trans Neural Netw Learn Syst, 2023, 34: 366–379
30 Xu H, Yu D, Sui S, et al. An event-triggered predefined time decentralized output feedback fuzzy adaptive control method for interconnected systems. IEEE Trans Fuzzy Syst, 2022, 31: 631–644
31 Hou Z, Xiong S. On model-free adaptive control and its stability analysis. IEEE Trans Automat Contr, 2019, 64: 4555–4569
32 Hui Y, Chi R, Huang B, et al. Extended state observer-based data-driven iterative learning control for permanent magnet linear motor with initial shifts and disturbances. IEEE Trans Syst Man Cybern Syst, 2021, 51: 1881–1891
33 Meng D, Zhang J. Robust optimization-based iterative learning control for nonlinear systems with nonrepetitive uncertainties. IEEE CAA J Autom Sin, 2021, 8: 1001–1014
34 Bu X, Jiang B, Lei H. Nonfragile quantitative prescribed performance control of waverider vehicles with actuator saturation. IEEE Trans Aerosp Electron Syst, 2022, 58: 3538–3548
35 Bu X, Qi Q, Jiang B. A simplified finite-time fuzzy neural controller with prescribed performance applied to waverider aircraft. IEEE Trans Fuzzy Syst, 2022, 30: 2529–2537
36 Dai S L, He S, Lin H, et al. Platoon formation control with prescribed performance guarantees for USVs. IEEE Trans Ind Electron, 2018, 65: 4237–4246
37 Zhu Y, Qiao J, Guo L. Adaptive sliding mode disturbance observer-based composite control with prescribed performance of space manipulators for target capturing. IEEE Trans Ind Electron, 2019, 66: 1973–1983

38 Liu Z, Lin W, Yu X, et al. Approximation-free robust synchronization control for dual-linear-motors-driven systems with uncertainties and disturbances. IEEE Trans Ind Electron, 2022, 69: 10500–10509
39 Zhang L, Che W W, Deng C, et al. Prescribed performance fuzzy resilient control for nonlinear systems under DoS attacks. IEEE Trans Syst Man Cybern Syst, 2023, 53: 3104–3116
40 Xu H, Yu D, Liu Y J. Observer-based fuzzy adaptive predefined time control for uncertain nonlinear systems with full-state error constraints. IEEE Trans Fuzzy Syst, 2024, 32: 1370–1382
41 Liu D, Zhou Z P, Li T S. Data-driven bipartite consensus tracking for nonlinear multiagent systems with prescribed performance. IEEE Trans Syst Man Cybern Syst, 2023, 53: 3666–3674
42 Wang Q, Jin S, Hou Z. Cooperative MFAILC for multiple subway trains with actuator faults and actuator saturation. IEEE Trans Veh Technol, 2022, 71: 8164–8174
43 Meng T, He W. Iterative learning control of a robotic arm experiment platform with input constraint. IEEE Trans Ind Electron, 2018, 65: 664–672
44 Freeman C T, Tan Y. Iterative learning control with mixed constraints for point-to-point tracking. IEEE Trans Contr Syst Technol, 2013, 21: 604–616
45 Chu B, Freeman C T, Owens D H. A novel design framework for point-to-point ILC using successive projection. IEEE Trans Contr Syst Technol, 2015, 23: 1156–1163
46 Shi S N, Li Y X. Event-based adaptive asymptotic tracking control of nonlinear time-varying systems with prescribed performance. J Control Decision, 2023, 10: 355–364
47 Liu D, Yang G H. Data-driven adaptive sliding mode control of nonlinear discrete-time systems with prescribed performance. IEEE Trans Syst Man Cybern Syst, 2019, 49: 2598–2604
48 Treesatayapun C. Prescribed performance of discrete-time controller based on the dynamic equivalent data model. Appl Math Model, 2020, 78: 366–382
49 Bu X, Yu W, Yu Q, et al. Event-triggered model-free adaptive iterative learning control for a class of nonlinear systems over fading channels. IEEE Trans Cybern, 2022, 52: 9597–9608
50 Lin N, Chi R, Huang B, et al. Event-triggered nonlinear iterative learning control. IEEE Trans Neural Netw Learn Syst, 2021, 32: 5118–5128
51 Ye D, Chen M M, Yang H J. Distributed adaptive event-triggered fault-tolerant consensus of multiagent systems with general linear dynamics. IEEE Trans Cybern, 2019, 49: 757–767
52 Ma Y, Che W, Deng C. Event-triggered model-free adaptive control for nonlinear cyber-physical systems with false data injection attacks. Intl J Robust NOnlinear, 2022, 32: 2442–2452
53 Su S, Li X, Tang T, et al. A subway train timetable optimization approach based on energy-efficient operation strategy. IEEE Trans Intell Transp Syst, 2013, 14: 883–893
54 Raghappriya M, Kanthalakshmi S. Sliding mode observer-based fault detection for helicopter system. J Control Decision, 2023, 10: 465–475
55 Liu G, Hou Z. Cooperative adaptive iterative learning fault-tolerant control scheme for multiple subway trains. IEEE Trans Cybern, 2022, 52: 1098–1111
56 Bu X, Yu Q, Hou Z, et al. Model free adaptive iterative learning consensus tracking control for a class of nonlinear multiagent systems. IEEE Trans Syst Man Cybern Syst, 2019, 49: 677–686
57 Yu X, Hou Z, Polycarpou M M. Distributed data-driven iterative learning consensus tracking for nonlinear discrete-time multiagent systems. IEEE Trans Automat Contr, 2022, 67: 3670–3677
58 Hou Z, Chi R, Gao H. An overview of dynamic-linearization-based data-driven control and applications. IEEE Trans Ind Electron, 2017, 64: 4076–4090
59 Hua C, Qiu Y, Guan X. Event-triggered iterative learning containment control of model-free multiagent systems. IEEE Trans Syst Man Cybern Syst, 2021, 51: 7719–7726